energy&fuels

pubs.acs.org/EF

Article

Evolution and Interfacial Dynamics of Thin Electrolyte Films in Oil−Brine−Carbonate Rock Systems due to Chemical Equilibrium Disruptions

Bamikole J. Adeyemi,* Prashant Jadhawar,* and Lateef Akanji

Cite This: *Energy Fuels* 2023, 37, 175−190

Read Online

ACCESS | Metrics & More | Article Recommendations | Supporting Information

ABSTRACT: This study presents the interfacial dynamics of viscoelastic thin electrolyte films between crude oil and rock surface, by integrating the effects of salt type and concentrations into the nonlinear evolution equation for viscoelastic thin liquid films. Dimensionless interfacial tension (IFT) is calculated for crude oil−NaCl, Na_2SO_4, $MgCl_2$, $MgSO_4$, $CaCl_2$, and $CaSO_4$ interfaces. Subsequently, the interfacial dynamics of the electrolyte films (bulk phase) are evaluated at selected characteristic viscoelastic parameters and various exposure times. Results show that chloride salts of Na^+, Mg^{2+}, and Ca^{2+} have lesser deteriorating effects on thin-film integrity compared with sulfate salts of the same cations while the presence of 1000 ppm $MgCl_2$ proves to constitute the least barrier to the stability of thin films. Contact angle is the most critical parameter affecting film dynamics, followed by crude oil−brine interfacial tension and the viscosity of thin electrolyte films. The difference between the ζ-potentials calculated at the crude oil−brine interface and at the brine−rock interface is a major factor in determining the response of thin electrolyte films to perturbations. A large difference between the two values of ζ-potential at the interfaces leads to better resistance to perturbations. Evaluation of the interfacial dynamics of viscoelastic thin electrolyte films is, therefore, a reliable method to determine wettability alteration due to smart water effects.

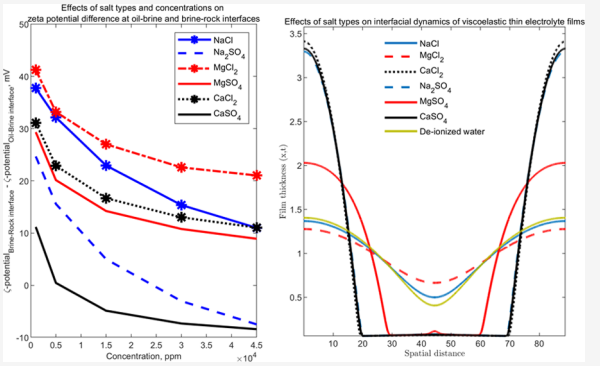

1. INTRODUCTION

Smart water flooding has received significant attention in the literature and it is very appealing to the oil and gas industry due to its lower capital intensity compared with other full-fledged enhanced oil-recovery (EOR) methods.[1] Several research studies have been conducted to investigate the effects of smart water in both sandstone and carbonate reservoirs. Most of the studies show that smart water injection has led to additional oil recovery.[2−7] In addition, improved oil recovery has been reported in the literature when smart water is co-injected with other EOR methods such as surfactants, polymers, and CO_2.[8]

Potential determining ions (Ca^{2+}, Mg^{2+}, SO_4^{2-}) present in injection and formation water, crude oil polar components, and reservoir mineralogy have been identified to be major contributors to smart water effects in reservoir systems.[4] Despite the current level of understanding of smart water EOR, the main challenge remains in the definition of the dominant mechanism behind the improved oil recovery associated with smart water injection.[1,7−10] Meanwhile, arguments on dominant mechanisms by various researchers are driven by specific findings under particular experimental conditions.

The uncertainty in defining the main mechanism behind smart waterflooding is mostly attributed to reservoir complexities when considered at the microscopic scale.[11] Hence, the oil and gas industry has conducted several field trials on smart waterflooding. Additional oil recovery from the trials shows that smart waterflooding requires more improvement to achieve its full potentials. Adequate knowledge of residual oil mobilization during smart waterflooding can unlock efficient and reliable design and deployment strategies required for greater oil recovery. Consequently, smart waterflooding is still considered to be an emerging EOR method, which requires extensive studies both at laboratory and field scales for effective design, deployment, and optimization. Crude oil mobilization from pore spaces is governed by thin-film dynamics, capillary forces, and intermolecular forces at the fluid−fluid and rock−fluid interfaces. The separation between these interfaces is marked by a potential profile caused by double-layer expansion as a result of the change in injection water chemistry.[8] There is, however, no existing direct experimental or mathematical

Received: July 28, 2022
Revised: November 21, 2022
Published: December 15, 2022

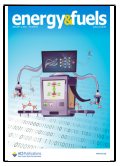

https://doi.org/10.1021/acs.energyfuels.2c02513
Energy Fuels 2023, 37, 175−190

approach that can be used to describe the dynamics of thin liquid films due to smart water effects in crude oil−brine−rock systems while considering the two mathematical interfaces.

Wettability alteration has mostly been described as the major contribution of smart water injection to increased oil recovery. Hence, the wettability of prescribed systems is deduced by estimating the contact angle at three-phase contact lines. The main effects of smart water, which lead to wettability alteration include brine−oil emulsification, wetting, and dewetting of the surface by oil, oil droplet drag, and snap-off suppression. These mechanisms are all affected by interfacial stability of the thin liquid film bound by oil−brine and brine−rock interfaces and the interfacial film stability is in turn controlled by the ionic concentration and interactions. Therefore, any method used to determine the smart water effect must capture the influence of rock mineralogy, pressure and temperature, salinity, pH, and the oil interfacial properties. The effect of any change in the mentioned factors on the wettability can be assessed by analyzing the stability of the thin water film between the rock surface and the bulk of the oil phase. Hence, evaluation of thin liquid film stability is the most reliable means by which smart water effects can be adequately captured.

The only approximate qualitative method available to relate thin-film dynamics to smart water effects is through the deduction of wettability changes by estimating the contact angle at three-phase contact lines using Derjaguin, Landau, Verwey, and Overbeek (DLVO) related techniques. While DLVO and related theories focus on the impact of interfaces on wettability alteration, the dynamics within the thin electrolyte films are much neglected. Meanwhile, recent findings have shown that additional oil recovery during smart waterflooding can be linked to the interfacial viscoelasticity of the thin electrolyte films.[12] Hence, formulations of a reliable mathematical model for describing smart water effects should include the integration of the interactions at the crude oil−brine and brine−rock interfaces, and the dynamics within thin electrolyte films in response to disruption in equilibrium of the reservoir system. The main purpose of this study is to investigate the interfacial behavior of the thin liquid film bound by the oil−brine and brine−rock interfaces to gain insight into the mechanism of smart water effects in carbonate reservoirs.

The stability of thin liquid films is an important aspect of wetting and dewetting of the rock surface by oil during crude oil mobilization from reservoirs.[13] Oil can be prevented from adhering to the rock surface if the thin liquid film is stable but unstable liquid film will lead to the rock surface becoming oil-wet or mixed-wet. Thin liquid films lying over-reactive rock surfaces are constantly under disjoining pressure which tends to increase the film thickness when positive but can lead to the attraction of crude oil to the rock surface if negative.[14] The impact of the two mathematical interfaces, that is, oil−brine and brine−rock interfaces on the magnitude of disjoining pressure has been captured by various proposed expressions for calculating double-layer forces covered in Derjaguin, Landau, Verwey, and Overbeek (DVLO).[15−27]

Preserving the stability of thin liquid films entails adequate understanding of the complexity of the interfacial microstructure as it relates to the interactions of surface active agents at the fluid−fluid interface, fluid−rock interface, and the bulk aqueous phase. The microstructures can lead to complex rheology of interfaces and thereby influence wetting and dewetting dynamics of such thin films.[11,28] One major interfacial property which strengthens thin-film stability is viscoelasticity and Sheng[6] concluded that salinity has significant effects on interfacial elasticity and viscous and elastic moduli. The importance of specific ions such as sodium (Na^+), magnesium (Mg^{2+}), calcium (Ca^{2+}), and sulfates (SO_4^{2-}), the viscoelasticity of the interfacial film was studied by Tang and Morrow.[7] The authors reported that stronger interfacial films due to increased viscous and elastic properties were observed with SO_4^{2-} ions while Ca^{2+} had a deteriorating effect on the films. A similar observation was made by McGuire et al.,[2] who concluded that viscoelasticity of the interfacial film is linked with improved snap-off suppression.

Zhang and Morrow[3] reported the roles of asphaltenes and organic acids on viscoelastic properties of interfacial films between crude oil and brine. The authors suggested the need for the integration of viscoelasticity with other parameters (wettability, fluid distributions, and mobility control), which might contribute to residual oil mobilization during smart waterflooding, Zhang et al.[4] reported increased viscoelasticity with decreased ionic strength of the aqueous phase. Al-Shalabi and Sepehrnoori[29] identified the role of sulfate ions in increasing the viscoelastic properties of interfacial films. The authors conducted coreflooding and interfacial rheology experiments with sulfate-rich smart water. Ding and Rahman[8] reported the impact of changes in the connectivity of the nonwetting phase on relative permeability and ultimate oil recovery. The importance of nonwetting phase connectivity and coalescence of oil ganglion has also been substantiated by RezaeiDoust et al.[9] Double-layer expansion is a proposed mechanism behind smart water effects, which integrates the different aspects of interfaces in oil/brine/rock systems.[10] The electric surfaces vary with ionic strength, pH, and ionic composition, and cannot be explained by simple adsorption models.[30] Thus, surface complexation models (SCMs) are applied in modeling the chemical interactions that accompany smart water injection into crude oil reservoirs and the electrical potential that develops between a charged surface and aqueous solutions.[31−54] SCM takes into consideration both adsorption onto surfaces and the electric double-layer (EDL) which is lacking in simple adsorption models.[55,56]

In this work, the viscoelastic thin-film evolution base model originally proposed by Rauscher et al.[57] and numerically solved by Barra et al.[58] is modified to accommodate the gradients of interfacial tension (IFT) that may occur in fluids with and without surface active agents or potential determining ions.[59] Integrating interfacial tension gradients with the original evolution equation for viscoelastic thin liquid films allows for the mathematical evaluation of the interfacial dynamics and the lubrication effects of thin electrolyte films bound by oil−brine and brine−rock interfaces in smart water-altered carbonate reservoirs.

The rest of the paper is organized as follows: The geometry of the problem and inclusion of the fluid−fluid interfacial effect into the nonlinear evolution equation for viscoelastic thin liquid films is discussed in Section 2. In Section 3, the estimation of dimensionless interfacial tension for the fluid−fluid interface is carried out. In Section 4, we present the simulation parameters used in this work. In Section 5, we perform the numerical simulations of the dynamic behavior of the system under different conditions. The correlation of the ζ-potential at the interfaces with interfacial dynamics of thin electrolyte films is presented in Section 6, and the conclusion drawn from the results of this study is presented in Section 7.

https://doi.org/10.1021/acs.energyfuels.2c02513
Energy Fuels 2023, 37, 175−190

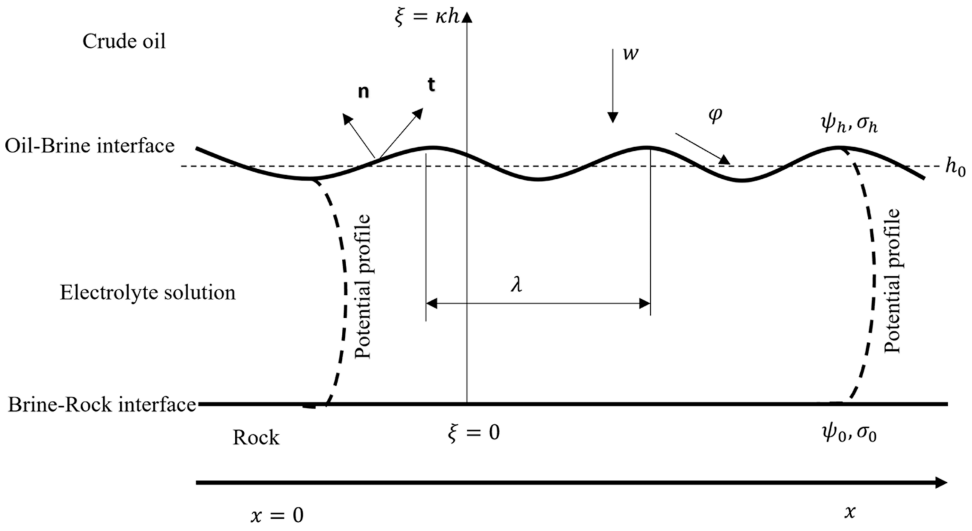

Figure 1. Schematics of the geometry of the research problem with the described thin electrolyte film bound above by crude oil−brine and below by brine−rock interfaces. The interfaces have potential, ψ_0 and ψ_h and charges, and σ_0 and σ_h for the brine−rock and the oil−brine interfaces, respectively. The prescribed forces (van der Waals, **w** and a tangential stress, φ) acting on the oil−brine interface are also shown.

2. GEOMETRY OF THE PROBLEM

Figure 1 defines the thin electrolyte film evaluated in this study. It consists of a system of viscoelastic thin electrolyte film subjected to perturbation by disjoining pressure. Disjoining pressure comprises three main forces, which are van der Waals force, structural force, and electric double-layer force. The geometry illustrates the schematic representation of the nondimensional potential profile between two charged plates combined with fluid interfaces and boundary conditions. There exist surface potentials at the two mathematical (oil−brine and brine−rock) interfaces and the separation between the interfaces is marked with potential profiles, which are a function of the ionic interactions and adsorption of surface reactive components in crude oil (acidic and basic contents), brine (cations and anions), and the carbonate rock (calcite and carbonates). Hence, the geometry presented here is representative of the thin electrolyte film sandwiched by oil and rock. The stability of the film is under disjoining pressure and it is controlled by exposure time, salt type, and concentrations.

The ionic interactions at the interfaces lead to the ζ-potential ψ_0 at the brine−rock interface and ψ_h at the crude oil−brine interface. The two interfaces are separated by dimensionless thickness $\xi = 0$ and $\xi = \kappa h$, where, κ [m^{-1}] is the reciprocal of Derby length and h [m] is the distance between them. The charges at both interfaces are represented by σ. The longitudinal direction is denoted by x, the transverse direction by y, and the respective velocity components by u and v. The liquid film is assumed to be thin enough, and van der Waals forces are effective and strong enough that a continuum theory of the liquid is applicable. The thin electrolyte film is subject to an external disjoining pressure, **w**, and a tangential stress, φ.

At equilibrium, the sum of the surface forces in the described geometry should balance out i.e equals to zero. The balance is disturbed by ionic interactions that occur when the chemistry of the system is altered e.g., injection of smart water. The physicochemical interactions caused by the variation in the ionic composition of the system can lead to a shift in the wetting condition of the rock surface. A change in the wettability of any particular rock surface is determined by contact angle measurements. Factors that affect the contact angle and therefore, wettability include pressure and temperature,[60−64] rock mineralogy,[30,65,66] pH,[67,68] salinity,[60,64,69−73] and the surface reactive components mostly reported as total acid number (TAN) and total base number (TBN).[68] Changes in these factors can be investigated by analyzing the stability of the thin liquid film.[14,74] The augmented Young−Laplace equation is used to assess the stability of liquid films bound by surfaces that deviate from ideal solid surfaces, represented by the following equation

$$P_c = \Pi^T + 2\sigma_{ow}H \tag{1}$$

where P_c [Pa] and Π^T are respectively the capillary pressure and the total disjoining pressure. σ_{ow} [N m^{-1}] is the interfacial tension (IFT) between wetting and nonwetting phases and H [m^{-1}] is the mean surface curvature of the droplet.

Total disjoining pressure, $\Pi^T(h)$ [Pa] at any particular thin liquid film thickness, h, is the sum of all the intermolecular forces i.e., van der Waals forces, Π^{vdW} [Pa], electric double-layer forces, Π^{EDL} [Pa], and structural forces, Π^{STR} [Pa]. The first two forces are referred to as Derjaguin, Landau, Verwey, and Overbeek (DLVO) theory,[75−77] while the last one is usually explained as non-DLVO theory. The total disjoining pressure is therefore estimated by

$$\Pi^T = \Pi^{vdW} + \Pi^{EDL} + \Pi^{STR} \tag{2}$$

Equation 2 shows that the stability of thin liquid films depends on the competition between the repulsive and attractive forces originating from disjoining pressure. Disjoining pressure is zero if it is equal to the capillary pressure, repulsive if it is positive, and attractive if it is negative. Estimation of disjoining pressure is used to predict the wettability of surfaces. The link between disjoining pressure and wettability is expressed as a measure of contact angle,[78] which can be predicted using the augmented Young−Laplace equation given as

https://doi.org/10.1021/acs.energyfuels.2c02513
Energy Fuels 2023, 37, 175−190

$$\cos\theta = 1 + \frac{1}{\sigma_{\alpha\beta}}\int_0^{P_c} h\mathrm{d}\Pi$$
$$= 1 + \frac{1}{\sigma_{\alpha\beta}}\left[P_c h(P_c) - \int_0^{h(P_c)} \Pi^T \mathrm{d}h\right] \quad (3)$$

where $\alpha\beta$ is the oil/water interface and $h(P_c)$ [m] is the film thickness at capillary pressure, P_c.

Equation 3 illustrates that changes in wettability of the oil−brine−rock system is altered by factors such as oil−brine interfacial tension, change in equilibrium thin liquid film thickness, and variations in disjoining pressure across the thin liquid film. DLVO theory has been applied as a tool for evaluating various processes such as adsorption at interfaces[15−18] and colloidal instability[19] by considering intermolecular forces as the basis for the mechanisms responsible for smart water effects during enhanced oil recovery.[8,20−26]

Contact angle estimation based on DLVO theory and the augmented Young−Laplace equation cannot, however, exactly match the experimental data even though DLVO theory can be applied to conduct the quantitative analysis of smart water effects on wettability change in oil/brine/rock systems.[79] In this work, the focus is, therefore, shifted to the changes in the oil−brine interfacial behavior and the dynamics of the thin electrolyte film, instead of using wettability alteration through contact angle prediction to analyze the smart water effect. Hence, experimentally measured equilibrium contact angles, θ_e, is included directly in a disjoining pressure, Π^T, expression which has been applied to thin liquid films of this nature[58,80−82]

$$\Pi^T(h) = \frac{\sigma(1-\cos\theta_e)}{Nh_*}\left[\left(\frac{h_*}{h}\right)^{n_1} - \left(\frac{h_*}{h}\right)^{n_2}\right] \quad (4)$$

$$N = \frac{(n_1 - n_2)}{](n_1 - 1)(n_2 - 1)]} \quad (5)$$

where n_1 and n_2 are constants such that $n_1 > n_2 > 1$. Several values of (n_1, n_2) have been studied in the literature and (3, 2), which have been widely used,[58,80−82] are chosen for this work. σ and h_* are the interfacial tension and the short length scale introduced by the van der Waals potential, respectively. In this form, the contribution of the electric double-layer force to total disjoining pressure is captured in the measured equilibrium contact angle, the interfacial tension, equilibrium thin-film thickness, and resulting thin-film thickness.

The dynamics of the thin films (shown as electrolyte solution in eq 1) bound by the crude oil−brine and brine−rock interfaces is, therefore, evaluated by applying the modified nonlinear evolution equation for viscoelastic thin films presented and numerically solved in our earlier study.[83] The dimensionless nonlinear evolution equation for viscoelastic thin films[57] is given as

$$\left(1 + \lambda_2\frac{\partial}{\partial t}\right)\frac{\partial h}{\partial t} + \frac{\partial}{\partial x}\left\{(\lambda_2 - \lambda_1)\left(\frac{h^2}{2}Q - hR\right)\frac{\partial h}{\partial t} + \left[\left(1 + \lambda_1\frac{\partial}{\partial t}\right)\frac{h^3}{3} + \left(1 + \lambda_2\frac{\partial}{\partial t}\right)bh^2\right]\frac{\partial}{\partial x}\left(\frac{\partial^2 h}{\partial x^2} - W(h)\right)\right\} = 0 \quad (6)$$

where, for compactness, Q, and R have been used such that

$$\left(1 + \lambda_2\frac{\partial}{\partial t}\right)Q = -\frac{\partial}{\partial x}\left(\frac{\partial p}{\partial x}\right) \quad (7)$$

$$\left(1 + \lambda_2\frac{\partial}{\partial t}\right)R = -h\frac{\partial}{\partial x}\left(\frac{\partial p}{\partial x}\right) \quad (8)$$

where λ_1 and λ_2 are the relaxation and retardation characteristic times, respectively. W is the dimensionless van der Waals induced by disjoining pressure, h is the thin-film thickness, p is the capillary pressure, and b is the slip coefficient.

The effect of the fluid−fluid interface is, however, trivialized in eq 6. Hence, we define an expression for interfacial tension within the long wave approximation of the Navier−Stokes equation, with Jeffreys constitutive model for viscoelastic stresses, to allow the study of interfacial dynamics due to the influence of physical and chemical properties of crude oil/brine/rock systems.

The spatial variation of surfactant concentration, C, along the interfaces, which gives rise to interfacial shear stress is considered and the interfacial tension is assumed to decrease linearly with surfactant concentration,[84] so that

$$\Sigma = \Sigma_0 - M_s C \quad (9)$$

and

$$\Sigma_0 = \frac{\sigma_0 h_0}{\rho\nu^2} \quad (10)$$

is the dimensionless interfacial tension for the constant part of the interfacial tension, σ_0, at the equilibrium concentration, C_0, and M_s is the solution version of the Marangoni number, proportional to

$$M_s = -C_0\left(\frac{h_0}{\rho\nu^2}\right)\left(\frac{\partial\sigma}{\partial C}\right) \quad (11)$$

where we remind the reader that σ is the dimensional interfacial tension, and the dimensionless surfactant concentration is expressed as $C = C/C_0$. Hence, the dimensionless capillary pressure, p, can be expressed as

$$p = -(\Sigma_0 - M_s C)\left(\frac{\partial^2 h}{\partial x^2}\right) - W(h) \quad (12)$$

Hence, the parameters to be estimated before eq 6 can be applied are defined by eq 9.

Contrary to simplistic assumptions by previous investigators, model formulation in this work reveals that both the capillary and van der Waals components of the pressure term are affected by the properties of the thin film including the fluid−fluid interactions. The final nonlinear evolution equation, therefore, becomes

https://doi.org/10.1021/acs.energyfuels.2c02513
Energy Fuels 2023, 37, 175−190

$$\left(1 + \lambda_2\frac{\partial}{\partial t}\right)\frac{\partial h}{\partial t} + \frac{\partial}{\partial x}\left\{(\lambda_2 - \lambda_1)\left(\frac{h^2}{2}Q - hR\right)\frac{\partial h}{\partial t} + \left[\left(1 + \lambda_1\frac{\partial}{\partial t}\right)\frac{h^3}{3} + \left(1 + \lambda_2\frac{\partial}{\partial t}\right)bh^2\right]\frac{\partial}{\partial x}\left(\Sigma\frac{\partial^2 h}{\partial x^2} - W(h)\right)\right\} = 0 \quad (13)$$

3. DIMENSIONLESS INTERFACIAL TENSION CALCULATIONS

The system under consideration consists of six selected salt types from Lashkarbolooki et al.[85] with unperturbed thickness $h_0 = 1$. The density ρ, the kinematic viscosity ν, and the constant part of the interfacial tension σ_0 are collected from the literature. The dimensionless interfacial tension for the constant part of the interfacial tension is, therefore, calculated using eq 10.

The Marangoni number is calculated for each electrolyte using eq 11 by estimating the equilibrium concentration, C_0 from the reported concentration in Lashkarbolooki et al.[85] The gradient of interfacial tension with concentration, $\frac{\partial\sigma}{\partial C}$ is estimated by taking the slope of the plot of change in the reported interfacial tension with concentration. The dimensionless interfacial tension due to brine concentration is, therefore, calculated for each salt type.

The response of a viscoelastic liquid to deformation when considering Jeffreys model is characterized by the relaxation time, λ_1, and the retardation time, λ_2, which are related by

$$\lambda_2 = \lambda_1\frac{\nu_s}{\nu_s + \nu_p} \quad (14)$$

where ν_s and ν_p are, respectively, the viscosity of the Newtonian solvent and the polymeric solute, such that $\nu = \nu_s + \nu_p$. Noting that the ratio $\nu_r = \nu_s/\nu_s + \nu_p \leq 1$, we have $\lambda_1 \geq \lambda_2$.[57,86,87] It is also observed that within the Jeffreys model, the Maxwell viscoelastic model is recovered when $\lambda_2 = 0$, and a Newtonian fluid when $\lambda_1 = \lambda_2$.[58]

Defining the dimensionless interfacial tension within the nonlinear evolution equation requires that the individual components that make up the expression be estimated as mentioned earlier. The following subsections describe the calculations of each parameter that constitute the dimensionless interfacial tension (see eq 9) due to brine concentration for each salt type and concentration.

3.1. Constant Part of the Interfacial Tension, Σ_0. The system under consideration consists of a thin electrolyte film with unperturbed thickness, h_0, bound above by the crude oil−brine interface and below by the brine−rock interface. The density ρ, the kinematic viscosity ν, and the constant part of the interfacial tension, σ_0, are collected from the literature. The dimensionless interfacial tension for the constant part of the interfacial tension is, therefore, calculated for the selected salts from Lashkarbolooki et al.[85] using eq 10.

3.2. Marangoni Number, M_s. The Marangoni number is calculated for each electrolyte solution using eq 11 by estimating the equilibrium concentration, C_0, from the reported brine concentrations in Lashkarbolooki et al.[85] The gradient of interfacial tension with concentration, $((\partial\sigma)/(\partial C))$ is calculated by estimating the slope of the plot of change in the reported interfacial tension with concentration.

3.3. Dimensionless Concentration, C. The dimensionless concentration for the selected brine solutions is calculated by dividing the reported concentrations (1000, 5000, 15,000, 30,000, 45,000 ppm) in Lashkarbolooki et al.[85] by the equilibrium concentrations of the adsorbed cations at the crude oil−brine interface using PHREEQC (a chemical speciation software). The chemical evolution modeling to estimate ζ-potential and the amount of adsorbed cations at the crude oil-brine and brine-rock interfaces is presented in the Supporting Information.

3.4. Average Viscosity Estimation. The response of a viscoelastic liquid to deformation when considering the Jeffreys model is characterized by the relaxation time, λ_1, and the retardation time, λ_2, which are related by

$$\lambda_2 = \lambda_1\frac{\nu_s}{\nu_s + \nu_p} \quad (15)$$

where ν_s and ν_p are the viscosity of the Newtonian solvent and the polymeric solute respectively, such that

$$\nu = \nu_s + \nu_p \quad (16)$$

Noting that the ratio

$$\nu_r = \frac{\nu_s}{(\nu_s + \nu_p)} \leq 1 \quad (17)$$

So that $\lambda_1 \geq \lambda_2$.[57,86,87]

4. SIMULATION PARAMETERS

The parameters for estimating the constant part of the dimensionless interfacial tension are shown in Table 1. Lashkarbolooki et al.[85] measured the interfacial tension, σ_0, of crude oil with a kinematic viscosity of 0.2158 [$cm^2\ s^{-1}$] in

Table 1. Constant Parameters for the Simulations

parameter	symbol	best estimates	reference
equilibrium interfacial tension	σ_0	22.32 [dyn cm^{-1}]	85
initial contact angle	CA	18.9	85
kinematic viscosity of crude oil	ν_p	0.2158 [$cm^2\ s^{-1}$]	85
kinematic viscosity of deionized water	ν_s	0.01 [$cm^2\ s^{-1}$]	88
density of thin film	ρ	0.9979 [g cm^{-1}]	85
equilibrium thin-film thickness	h_0	10^{-6} [cm]	8
			89
			90
dimensionless interfacial tension	$\Sigma_0 = \sigma_0 h_0/\rho\nu_s^2$	0.2237	
interfacial tension variation, NaCl	$(\partial\sigma/\partial C)_{NaCl}$	−0.684	
interfacial tension variation, Na_2SO_4	$(\partial\sigma/\partial C)_{Na_2SO_4}$	−0.61	
interfacial tension variation, $MgCl_2$	$(\partial\sigma/\partial C)_{MgCl_2}$	−3.854	
interfacial tension variation, $MgSO_4$	$(\partial\sigma/\partial C)_{MgSO_4}$	−0.828	
interfacial tension variation, $CaCl_2$	$(\partial\sigma/\partial C)_{CaCl_2}$	−1.954	
interfacial tension variation, $CaSO_4$	$(\partial\sigma/\partial C)_{CaSO_4}$	3.651	

https://doi.org/10.1021/acs.energyfuels.2c02513
Energy Fuels 2023, 37, 175−190

Table 2. Estimated Dimensionless Brine Concentration, Marangoni Number, and Dimensionless Interfacial Tension Along with the Reported Measured Contact Angle (CA) for Na^+ Salts at Various Brine Concentrations

	NaCl				Na_2SO_4			
C [ppm]	$C = \frac{C}{C_0} \times 10^5$	$M_s \times 10^{-9}$	Σ	CA	$C = \frac{C}{C_0} \times 10^4$	$M_s \times 10^{-9}$	Σ	CA
1000	0.6547	1.7904	0.2236	18.80	0.5783	1.4800	0.2236	20.3
5000	1.4597	4.0338	0.2231	18.67	1.1943	3.5827	0.2233	19.9
15,000	2.9059	6.1470	0.2219	18.87	2.3246	5.5749	0.2224	20.0
30,000	4.6585	7.7866	0.2201	18.87	3.6947	7.0481	0.2211	20.0
45,000	6.2119	8.8970	0.2182	19.10	4.9042	7.9773	0.2198	20.0

Table 3. Estimated Dimensionless Brine Concentrations, Marangoni Number, and Dimensionless Interfacial Tension along with the Reported Measured Contact Angle (CA) for Mg^{2+} Salts at Various Brine Concentrations

	$MgCl_2$				$MgSO_4$			
C [ppm]	$C = \frac{C}{C_0} \times 10^5$	$M_s \times 10^{-8}$	Σ	CA	$C = \frac{C}{C_0} \times 10^5$	$M_s \times 10^{-9}$	Σ	CA
1000	0.3193	1.3305	0.2233	18.4	0.2574	2.5788	0.2236	19.4
5000	1.1255	1.8187	0.2217	22.7	0.9722	3.5845	0.2234	22.7
15,000	2.6730	2.2829	0.2176	23.7	2.3496	4.4142	0.2227	22.0
30,000	4.4947	2.7324	0.2114	24.7	4.0988	5.0407	0.2216	21.8
45,000	5.9547	3.1067	0.2052	24.6	5.6696	5.4589	0.2206	22.2

Table 4. Estimated Dimensionless Brine Concentration, Marangoni Number, and Dimensionless Interfacial Tension Along with the Reported Measured Contact Angle (CA) for Ca^{2+} Salts at Various Brine Concentrations

	$CaCl_2$				$CaSO_4$			
C [ppm]	$=\frac{C}{C_0} \times 10^5$	$M_s \times 10^{-8}$	Σ	CA	$C = \frac{C}{C_0} \times 10^4$	$M_s \times 10^{-8}$	Σ	CA
1000	0.2021	0.8720	0.2235	21.7	1.6655	−1.5377	0.2240	20.7
5000	0.7899	1.1155	0.2228	20.9	2.4315	−1.6552	0.2241	19.2
15,000	2.0160	1.3209	0.2210	20.8				
30,000	3.5831	1.49740	0.2183	21.9				
45,000	4.9712	1.63070	0.2156	22.1				

deionized water with kinematic viscosity of 0.01 [$cm^2\ s^{-1}$][88] to be 22.32 [dyn cm^{-1}]. A typical equilibrium thin-film thickness, h_0, has been reported to be about 10^{-6} [cm].[8,89,90] The density of the thin film at equilibrium, ρ, is assumed to be the density of the deionized water since the contributions of the crude oil to the total density are only at the interface and can be said to be negligible.

Variation of the interfacial tension with different electrolyte solution concentrations and compared with the experimental data reported in Lashkarbolooki et al.[85] Hence, the variation of interfacial tension, $(\partial\sigma/\partial C)$, for each salt type is estimated by finding the slope of the logarithmic trendline of the plots using Microsoft Excel.

The gradient of interfacial tension with salt concentration shows that the changes in interfacial tension are slower when the brine solutions are predominantly chloride salts compared to the changes observed when sulfate salts are used. The difference in the interfacial tension variation for Na^+ salts (NaCl and Na_2SO_4) is smaller when compared with Mg^{2+} salts ($MgCl_2$ and $MgSO_4$) and that of Ca^{2+} salts ($CaCl_2$ and $CaSO_4$). There is a downward trend of interfacial tension as indicated by the negative gradient numbers, which shows a reduction in the interfacial tension with salt concentrations. It is, however, difficult to make any generalization on the gradient of interfacial tension for $CaSO_4$ since the experiment was conducted for only two salt concentration values (1000 and 1500 ppm). Tables 2−4 show the estimated dimensionless salt concentrations, Marangoni number, and dimensionless interfacial tension for the selected salt types and concentrations.

5. DYNAMICS OF VISCOELASTIC THIN ELECTROLYTE FILMS

In this section, the numerical results for dewetting thin electrolyte films in response to the impact of disjoining pressure as constituted by van der Waals interactions are presented. The initial flat fluid interface of thickness $h_0 = 1$ is perturbed with $k = k_m$ and $\delta = 0.01$. The calculated domain size is 44.45 and an equilibrium film thickness $h_* = 0.05$. The set of parameters used for all simulations in this work including the dimensionless interfacial tension and measured equilibrium contact angles are shown in Tables 2−4. Other parameters remain as presented previously.

5.1. Validation. The numerical investigations are validated by comparing the growth rate for the early times with the linear stability analysis (LSA) of eq 6. Figure 2 shows the comparison of the computed growth rates for the wavenumber of the maximum growth rate with the one given by the dispersion relation $\omega(k)$, for a film with $\lambda_1 = 5$ and $\lambda_2 = 0.05$, when b= 0. For these numerical simulations, the domain size is chosen according to the wavelength that corresponds to the wavenumber of the maximum growth rate. Similar comparisons between the computed growth rate and LSA were made for all the simulations.

5.2. Base Case. The dynamics of the thin electrolyte films at three selected times are discussed, which describe the

https://doi.org/10.1021/acs.energyfuels.2c02513
Energy Fuels 2023, 37, 175−190

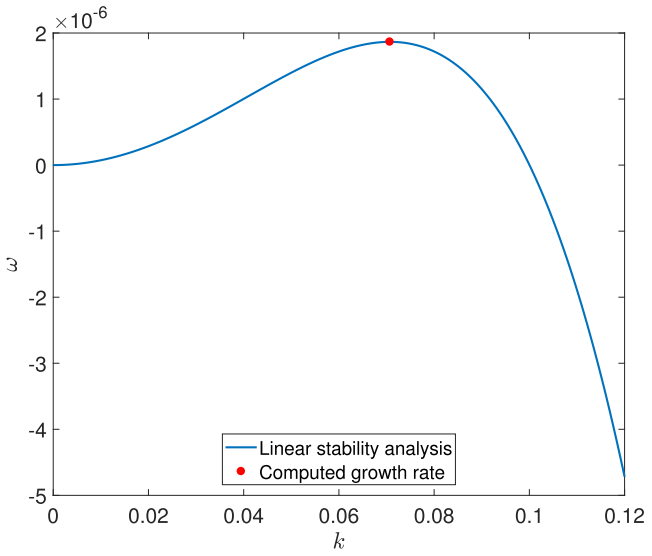

Figure 2. Comparison of the growth rate for the linear stability analysis compared with the computed growth rate of the numerical simulations at the wavelength of the maximum growth rate.

interfacial dynamics as being divided into three phases. Figure 3 shows three phases of the interfacial dynamics of the thin viscoelastic electrolyte film composed of deionized water (i.e., without any salt types), which serves as the base case. The initial phase corresponds to the short-time viscous response of the fluid before the film separates in two retracting rims (Figure 3a). In the intermediate phase, the fastest dynamics occurs and the response of the liquid is elastic, holes and retracting edges form in this regime (Figure 3b). During the last regime, the rims increase in height, until the interface reaches its final configuration, attaining an equilibrium contact angle with the solid surface (Figure 3c). During this third stage, the fluid shows a long-time Newtonian response again.

5.3. Effects of NaCl and Na_2SO_4. The response of the described viscoelastic thin electrolyte film to the prescribed perturbation caused by the van der Waals induced disjoining pressure using the reported contact angle is investigated at various concentrations of NaCl and Na_2SO_4. The spontaneous dewetting of the films is studied at the selected three phases described.

Figure 4 shows the dynamics of the films at various concentrations of NaCl at the three exposure time values. At the initial regime when $t = 1.45 \times 10^6$ (Figure 4a) and for all concentrations, separation of rims has started but not fully developed. The film dynamics is affected by the concentration of Na^+ within the thin film. The increase in the Na^+ concentration causes further bridging between the rock surface and the crude oil until it reaches an optimum level beyond which it deteriorates the stability of the film at the injection salinity of 45,000 ppm. The separation becomes faster and fully developed at the intermediate regime when $t = 1.59 \times 10^6$ (Figure 4b). There is also the formation of a retracting hole at this stage. Different growth rates are observed at different concentrations of the electrolyte with the film at 45,000 ppm of NaCl reaching the highest growth while the least growth is observed at 5000 ppm of NaCl. Therefore, the amount of Na^+ needed to support optimum double-layer expansion where the effect of disjoining pressure on the film is minimum is achieved at 5000 ppm. In the last phase of the film configuration (Figure 4c), all films irrespective of the electrolyte concentration reached the maximum growth and ruptured.

The van der Waals forces dominate the responses of the films to perturbation at the early stage of the film configuration since the film growth show dependence on the salinity of NaCl. This observation is in agreement with several experimental studies.[91] At this stage, the disjoining pressure is positive, which leads to higher attraction of the films to the surface as the concentration of NaCl increses but there are no observable significant contributions of the dimensionless interfacial tension. This trend continues until the intermediate regime when all the films develop further and some of them rupture. There are, however, some changes in the configuration of the films, which could be attributed to the effects of dimensionless interfacial tension. The film heights correspond to the reduction of dimensionless interfacial tension with the highest at a salinity of 45,000 ppm ($\Sigma = 0.2182$) and the lowest at a salinity of 1000 ppm ($\Sigma = 0.2236$). The dynamics at the intermediate regime correspond to the effects of various concentrations of NaCl on wettability changes and eventual additional oil recovery, which have been demonstrated in reported experimental studies.[91−95] In the last regime, there is no noticeable dominant factor that is responsible for the film behavior since all the films reach their maximum growth and attained approximately equal height and rupture.

Figure 5 shows the evolution and configurations of the viscoelastic thin electrolyte films formed at various concentrations of Na_2SO_4 at the three selected phases. Figure 5a shows that the films have fully developed and the rims already separated at the early time regime. The only observable differences in the configurations of the films according to salinity at this stage are the heights of the rims formed and the final growth of individual films. The rims quickly disappear and none can be noticed at the intermediate time regime but the difference in final growth reached by the films remains unchanged from the earlier stage (Figure 5b). There is no observable difference between the film configuration at the intermediate phase and the final regime at $t = 3.45 \times 10^6$ (Figure 5c).

The films formed between Na_2SO_4 and crude oil at various concentrations result in a higher contact angle and dimensionless interfacial tension. The dynamics of the films are faster than the ones for NaCl and reach the maximum height at the early regime. The only observable factor that suggests the contributions of individual determinants is the height of the hole formed during the separation of the rims. The film morphology in Figure 6a shows that the hole heights are dependent on the dimensionless interfacial tension. Even though the films proceed at approximately the same rate, the maximum height attained slightly vary, which indicates the influence of the dimensionless interfacial tension. These observations are in agreement with experimental results where the presence of SO_4^{2-} with brine solution could not yield any significant additional oil recovery.[9]

5.4. Effects of $MgCl_2$ and $CaCl_2$. The dynamics of the dewetting films developed when $MgCl_2$ is used at the five selected concentrations are shown in Figure 6. All the films except the one at 1000 ppm $MgCl_2$ have fully developed and the rims separated at the early phase of the film configuration (Figure 6a). There is no difference in the film growth by the time the dynamics gets to the intermediate phase of the film configuration but all the films except the one at 1000 ppm have ruptured, as shown in Figure 6b. At the last time regime

https://doi.org/10.1021/acs.energyfuels.2c02513
Energy Fuels 2023, 37, 175−190

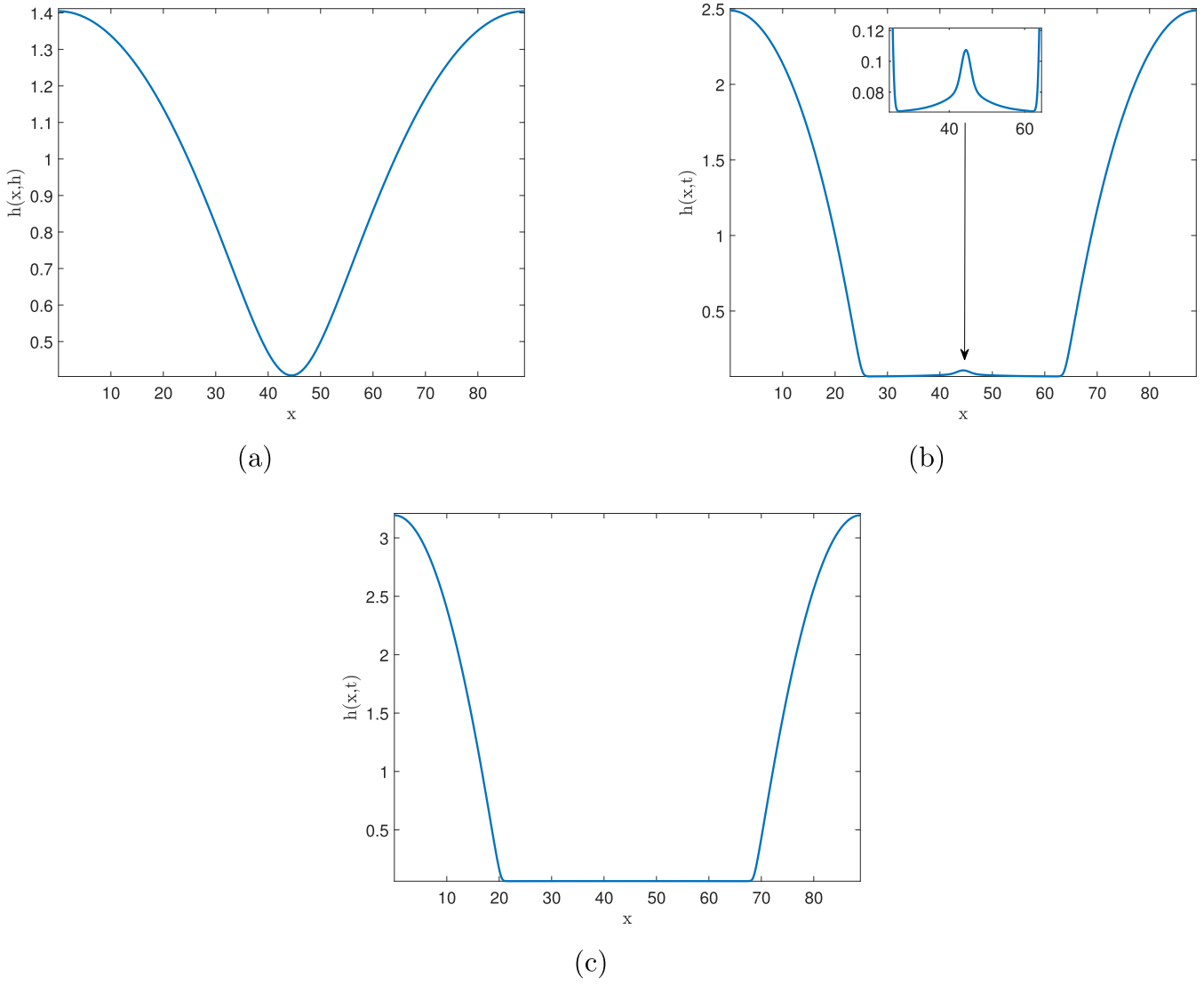

Figure 3. Evolution of three distinct films with $\lambda_1 = 5$, $\lambda_2 = 1$, $h_0 = 1$, and $h_* = 0.05$ showing the dynamics at three selected times (a) $t = 1.45 \times 10^6$ (b) $t = 1.59 \times 10^6$, and (c) $t = 3.45 \times 10^6$. The inset in (b) shows a close-up of the separating rim formed in the intermediate regime before the final configuration shown in (c).

(though not shown here for brevity), all the films, including the film at 1000 ppm $MgCl_2$ concentration, reached their maximum growth and ruptured.

It is interesting to note that the strongest film is developed at the highest dimensionless interfacial tension. Hence, the dominance of the contact angle is demonstrated in the responses of crude oil-$MgCl_2$ film to the prescribed perturbation regardless of the values of dimensionless interfacial tension. There is, however, an inverse relationship between the dimensionless interfacial tension and the measured contact angle with salinity. Taheriotaghsara et al.[79] explained the increasing contact angle and the decreasing interfacial tension with $MgCl_2$ concentration by suggesting that the reduction in interfacial tension leads to improved spreading, which enables the oil to occupy a larger area on the rock surface, resulting in less water-wetness. Similar observations have been made somewhere else.[68,96] It follows from here that an optimum interfacial tension could be sought to preserve the integrity of thin liquid films.

Figure 7 shows the evolution and dynamics of two distinct dewetting films developed for various concentrations of $CaCl_2$ electrolyte solutions. At the early stage of the film configuration (Figure 7a), all the films have already fully developed and rims fully separated with formation of a hole each. The films at the end of the early time regime show a similar growth rate. There are no observable differences in the growth rate and maximum film height at the intermediate regime (Figure 7b), except for the fact that the rims have disappeared. These observations are similar to the ones for $MgCl_2$ electrolyte films in configurations but the film growth in $MgCl_2$ is higher and the film at 1000 ppm salt concentration is not fully developed even at the intermediate time regime.

5.5. Effects of $MgSO_4$ and $CaSO_4$. The responses of the thin films to perturbations due to the effects of sulfate salts of Mg^{2+} and Ca^{2+} are shown and discussed in this section. The evolution and dynamics of the dewetting films with $MgSO_4$ as shown in Figure 8a proceed very fast at the initial time regime just as described for $MgCl_2$ but with a more developed film at 1000 ppm salt concentration. There is formation of a hole in the film at 1000 ppm showing that the film is greatly impacted by the prescribed force in this case. At the middle stage of the film dynamics (shown in Figure 8b), the hole has disappeared

https://doi.org/10.1021/acs.energyfuels.2c02513
Energy Fuels 2023, 37, 175−190

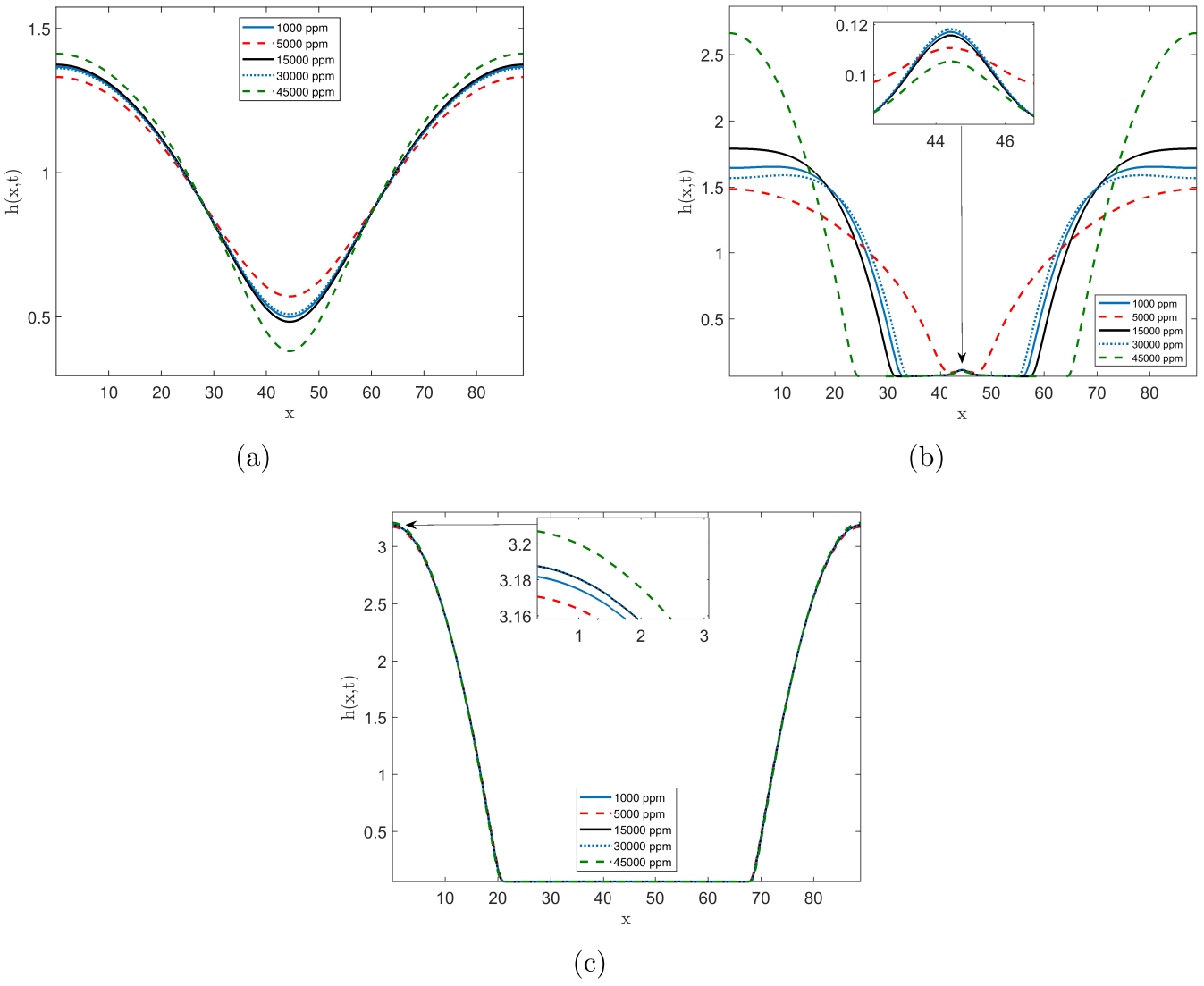

Figure 4. Evolution of dewetting films with $\lambda_1 = 5$, $\lambda_2 = 1$, $h_0 = 1$, and $h_* = 0.05$ for various concentrations of NaCl at (a) $t = 1.45 \times 10^6$, (b) $t = 1.59 \times 10^6$, and (c) $t = 3.45 \times 10^6$. The insets in (b) and (c) show a close-up of the separation of the developed rims in the intermediate regime and the maximum film growth in the last phase of the film configuration, respectively.

and the film has grown further and ruptured like every other film at higher salt concentration. There is no observable further development or changes in the film configuration after the intermediate phase, and hence, the results is not shown here for brevity. The dynamics of the film at the 1000 ppm concentration of $MgSO_4$ shows an agreement with experimental observation where Chandrasekhar and Mohanty[97] and Chandrasekhar et al.[38] measured the contact angle on oil-wet calcite and concluded that modified seawater containing Mg^{2+} and SO_4^{2-} could lead to wettability alteration to more water-wet conditions.

Figure 9 shows the dynamics of two distinct dewetting films at 1000 and 1500 ppm of $CaSO_4$ electrolyte solution at two of the three selected time regimes (the final stage of the film configuration is not shown since there is no observable difference between it and the intermediate stage). At the early phase of the film configuration shown in Figure 9a, the film with lower salinity is already fully developed and ruptured while the other film with higher salinity is merely developed with separated rims and formation of a hole. By the intermediate regime (Figure 9b), both films have fully developed and ruptured with the film of lower salinity having a higher film height.

6. CORRELATION OF THE ζ-POTENTIAL AT THE INTERFACES WITH INTERFACIAL DYNAMICS OF THE THIN FILMS

The impact of salt type and concentrations on ζ-potentials at both the crude oil−brine and brine−rock interfaces, and concentrations of cations in the formation water are discussed in this section. Figure 10 shows the effects of chloride and sulfate salts of Na^+ on the calculated ζ-potential at crude oil−brine interface and brine−rock interface. First, there is a relationship between the estimated ζ-potential at the brine−rock interface and the contact angle which shows that more negative or lower ζ-potential at the brine−rock interface results in a lower contact angle (Table 2). Second, the ζ-potential at both the crude oil−brine interface and brine−rock interface become more negative with Na_2SO_4 salt compared to NaCl salt. Conversely, there is an inverse relationship between the estimated ζ-potential at the crude oil−brine interface (Figure 10) and the calculated dimensionless interfacial (Table 2).

https://doi.org/10.1021/acs.energyfuels.2c02513
Energy Fuels 2023, 37, 175−190

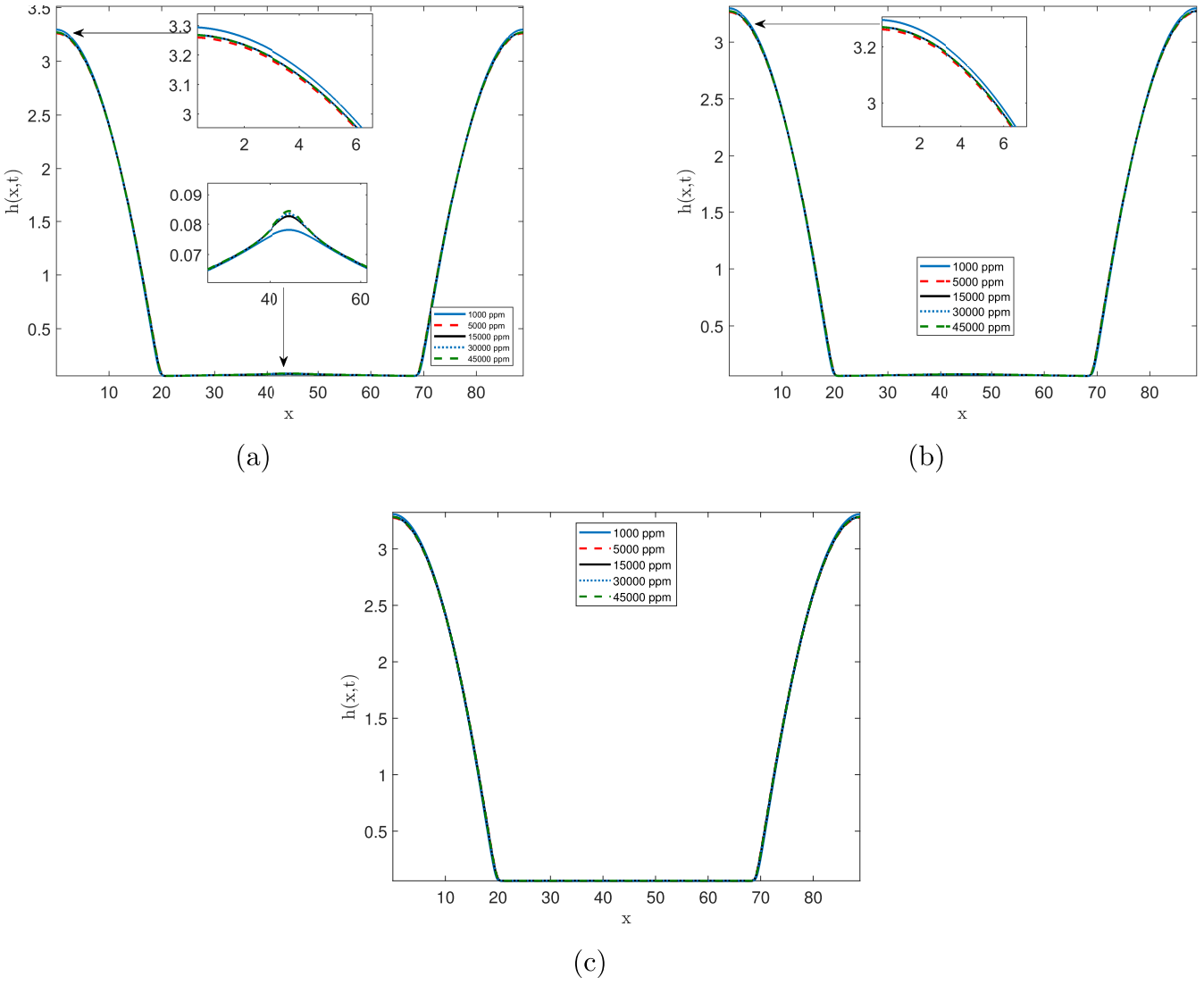

Figure 5. Evolution of dewetting films with $\lambda_1 = 5$, $\lambda_2 = 1$, $h_0 = 1$, and $h_* = 0.05$ for various concentrations of Na_2SO_4 at (a) $t = 1.45 \times 10^6$, (b) $t = 1.59 \times 10^6$, and (c) $t = 3.45 \times 10^6$. The insets in (a) show a close-up of the separation of the developed rims in the early regime and the maximum film growth in the last phase of the film configuration. The inset in (b) shows the region of maximum film height after rupturing.

To correlate the ζ-potential at both interfaces, the difference between the estimated ζ-potential values at both interfaces is compared with the dynamics of the thin electrolyte films, shown in Figures 4 and 5. There is a corresponding increase in the strength of thin electrolyte films with the differences in ζ-potential values at the interfaces. Thin films within the same salt type respond to perturbations according to the differences in ζ-potential values between the crude oil−brine interface and brine−rock interface. A higher difference in the ζ-potential leads to delayed film development and late rupture. The observed dissimilarity between the responses of the films of different salt types to perturbations can be explained by the force of attraction between the crude oil−brine interface and brine−rock interface caused by the presence of Cl^- and SO_4^{2-} in the bulk phase. The result of the dynamics simulation shows that SO_4^{2-} ions increase forces of adhesion more than the Cl ions.

Figure 11 shows the comparison of the estimated ζ-potentials at the crude oil−brine and brine−rock interfaces for chloride and sulfate salts of Mg^{2+} ions. Again, the presence of sulfate ions increases the negativity of ζ-potential. With reference to Table 3, while there is a direct relationship between the estimated ζ-potential of the $MgCl_2$ brine−rock interface and the contact angle, however, there is no relationship between ζ-potential and contact angle at the $MgSO_4$ brine−rock interface. Meanwhile, there is a direct relationship between the ζ-potential at the crude oil−brine interface and dimensionless interfacial tension for both salt types (i.e., $MgCl_2$ and $MgSO_4$) in which dimensionless interfacial tension decreases with increasing ζ-potential.

To correlate the ζ-potential at both interfaces, the difference between the estimated ζ-potential values at both interfaces is compared with the dynamics of the thin electrolyte films shown in Figures 6 and 8. For $MgCl_2$, there is a corresponding increase in the strength of thin electrolyte films with the differences in ζ-potential values at the interfaces. Thin films within the same salt type respond to perturbations according to the differences in ζ-potential values between the crude oil−brine interface and the brine−rock interface. A higher difference in the ζ-potential leads to delayed film development and late rupture.

https://doi.org/10.1021/acs.energyfuels.2c02513
Energy Fuels 2023, 37, 175−190

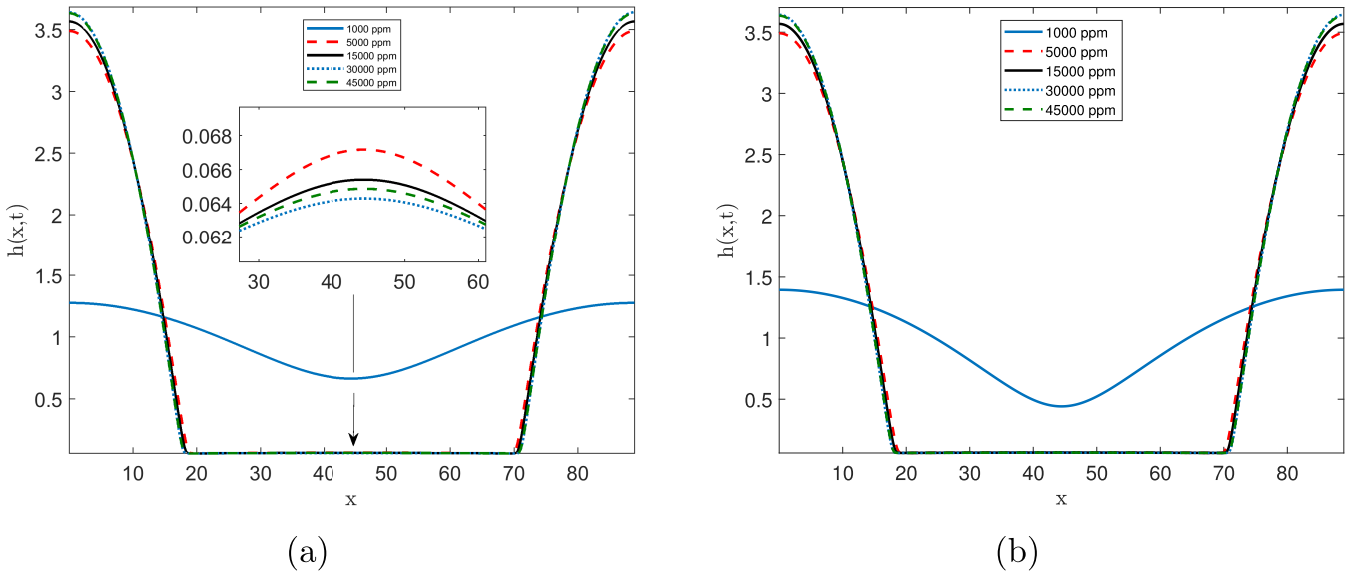

Figure 6. Evolution of dewetting films with $\lambda_1 = 5$, $\lambda_2 = 1$, $h_0 = 1$, and $h_* = 0.05$ for various concentrations of $MgCl_2$ at (a) $t = 1.45 \times 10^6$ and (b) $t = 1.59 \times 10^6$. The insets in (a) show a close-up of the separation of the developed rims in the early regime and the maximum film growth in the last phase of the film configuration. The inset in (a) shows the close-up of the region of rim separation with the holes formed by the films at individual electrolyte concentrations.

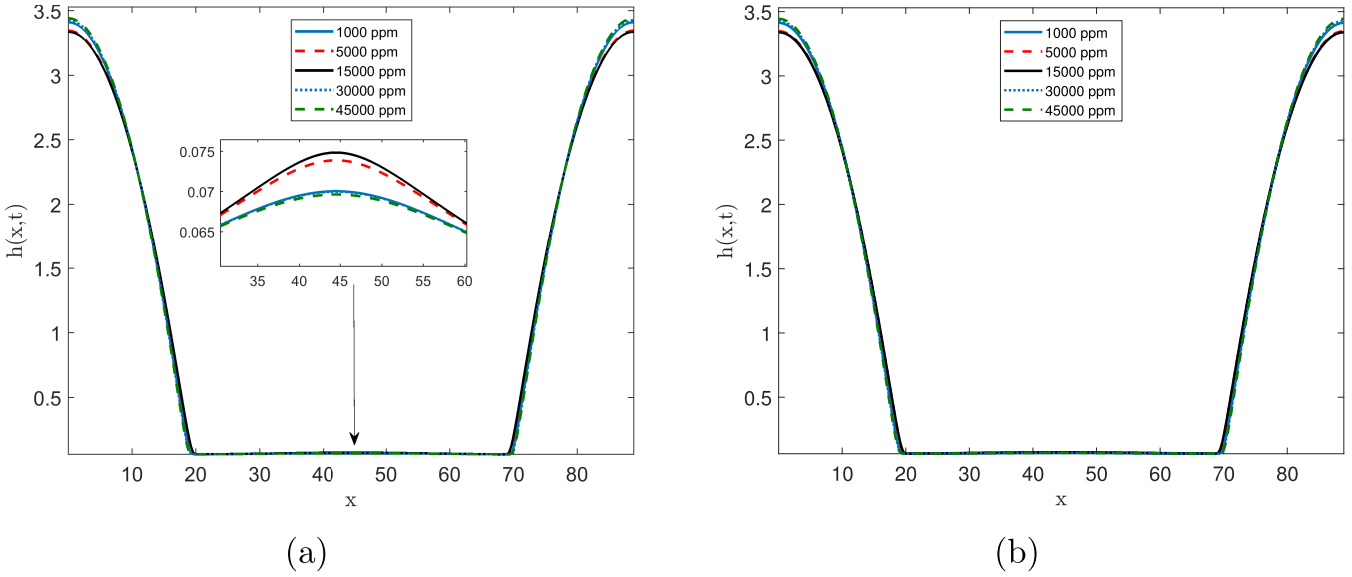

Figure 7. Evolution of dewetting films with $\lambda_1 = 5$, $\lambda_2 = 1$, $h_0 = 1$, and $h_* = 0.05$ for various concentrations of $CaCl_2$ at (a) $t = 1.45 \times 10^6$ and (b) $t = 1.59 \times 10^6$. The insets in (a) show a close-up of the separation of the developed rims in the early regime and the maximum film growth in the last phase of the film configuration. The inset in (a) shows the close-up of the region of rim separation with the holes formed by the films at individual electrolyte concentrations.

Figure 12 shows the effects of chloride and sulfate salts of Ca^{2+} on the calculated ζ-potential at the crude oil−brine interface and brine−rock interface. The estimated ζ-potential at the interfaces becomes more negative upon the injection of $CaSO_4$ compared to when $CaCl_2$ was injected. There is no observable correlation between the thin-film dynamics and the estimated ζ-potential at the interfaces.

7. CONCLUSIONS

The nonlinear evolution for viscoelastic thin electrolyte films developed in this study involves the definition of the modified expression for interfacial tension within the long wave approximation of the Navier−Stokes equation, with the Jeffreys constitutive model for viscoelastic stresses. Integration of the dimensionless interfacial tension into the evolution equation for viscoelastic thin electrolyte films allows the study of interfacial dynamics due to the influence of physical and chemical properties of crude oil/brine/rock systems. The constant part of the dimensionless interfacial tension constitutes the physical properties of the thin electrolyte films while the product of the Marangoni number and the cation concentration forms the chemical component of the dimensionless interfacial tension. Hence, only the Marangoni number aspect of dimensionless interfacial tension is altered by changes in injection water chemistry.

https://doi.org/10.1021/acs.energyfuels.2c02513
Energy Fuels 2023, 37, 175−190

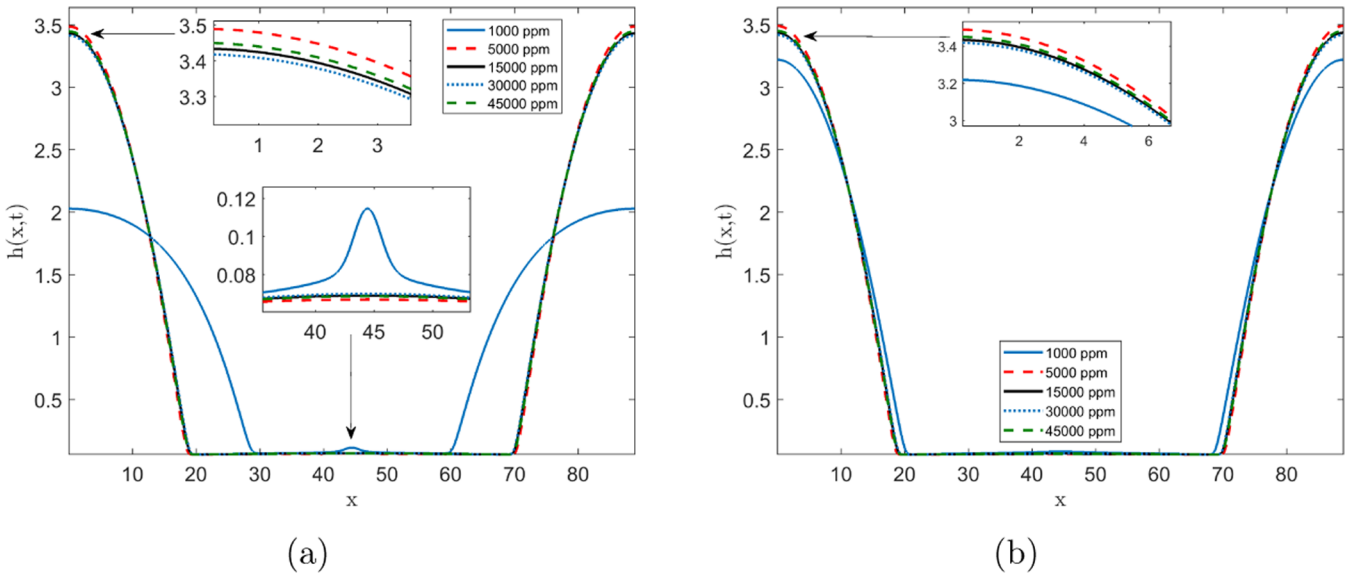

Figure 8. Evolution of dewetting films with $\lambda_1 = 5$, $\lambda_2 = 1$, $h_0 = 1$, and $h_* = 0.05$ for various concentrations of $MgSO_4$ at (a) $t = 1.45 \times 10^6$ and (b) $t = 1.59 \times 10^6$. The insets in (a) show a close-up of the separation of the developed rims in the early regime and the maximum film growth in the last phase of the film configuration. The inset in (b) shows a close-up of the region of maximum film height after rupturing.

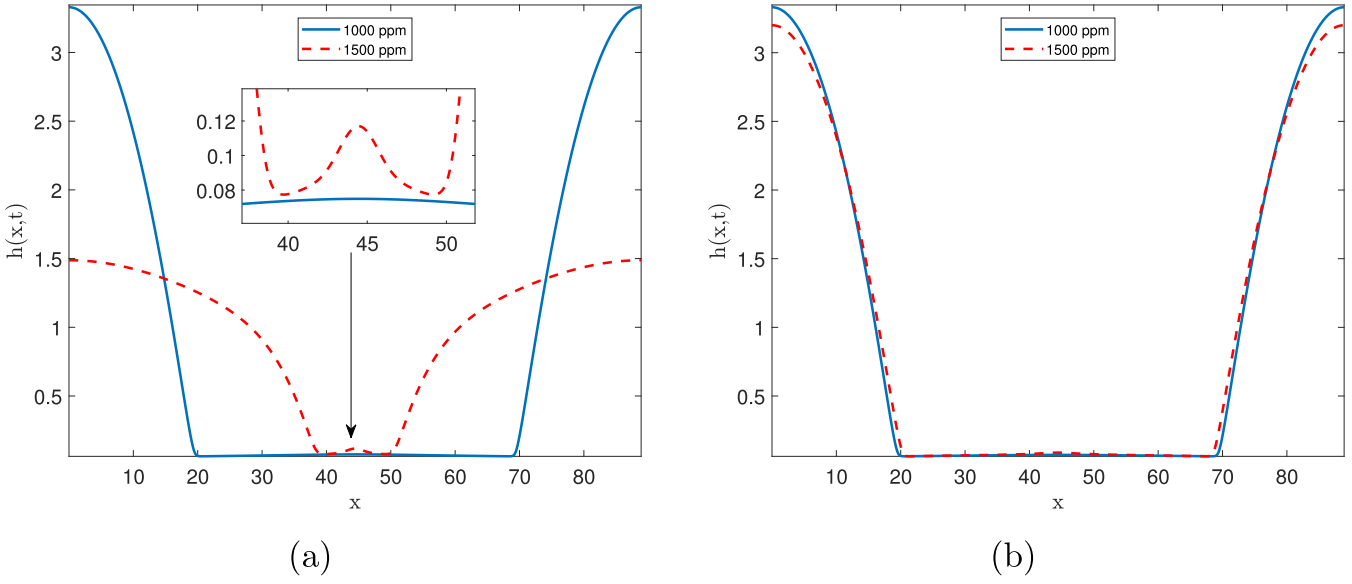

Figure 9. Evolution and dynamics of dewetting films with $\lambda_1 = 5$, $\lambda_2 = 1$, $h_0 = 1$, and $h_* = 0.05$ for 1000 and 1500 ppm of $CaSO_4$ at (a) $t = 1.45 \times 10^6$ and (b) $t = 1.59 \times 10^6$. The inset in (a) shows a close-up of the separation of the developed rims in the early regime.

Dimensionless interfacial tension is calculated for NaCl, Na_2SO_4, $MgCl_2$, $MgSO_4$, $CaCl_2$, and $CaSO_4$. The effects of these electrolytes and their concentrations on the film dynamics are evaluated using the modified thin-film evolution equation developed in this study at three time regimes. The destabilizing effects of adding Ca^{2+} on the dynamics of the viscoelastic thin electrolyte films are stronger than that of Mg^{2+} and Na^+, irrespective of the salt type. Viscoelastic thin electrolyte films with $MgCl_2$ exhibit the slowest dynamics. Effects of the salt type and concentrations on the values of the estimated ζ-potentials at the interfaces are investigated. The ζ-potential profiles reveal a correlation between charges at the mathematical interfaces and the interfacial dynamics of the thin electrolyte films. The larger the difference between the ζ-potential at the crude oil−brine and brine−rock interfaces, the stronger the viscoelastic thin electrolyte films and the longer it takes for the films to rupture.

■ ASSOCIATED CONTENT

Supporting Information

The Supporting Information is available free of charge at https://pubs.acs.org/doi/10.1021/acs.energyfuels.2c02513.

Chemical evolution modeling, surface complexation, cation exchange and adsorption, advection-transport calculations, chemical composition of the evolved thin electrolyte films, Figures S1−S6 (PDF)

https://doi.org/10.1021/acs.energyfuels.2c02513
Energy Fuels 2023, 37, 175−190

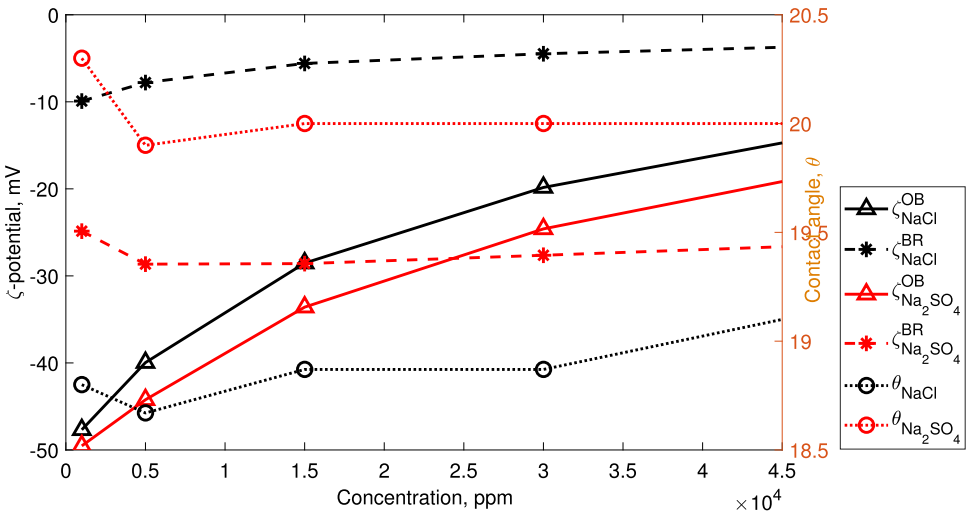

Figure 10. Calculated ζ-potential for chloride and sulfate salts of sodium ion (Na^+) at the crude oil–brine and brine–rock interfaces, as a function of salinity.

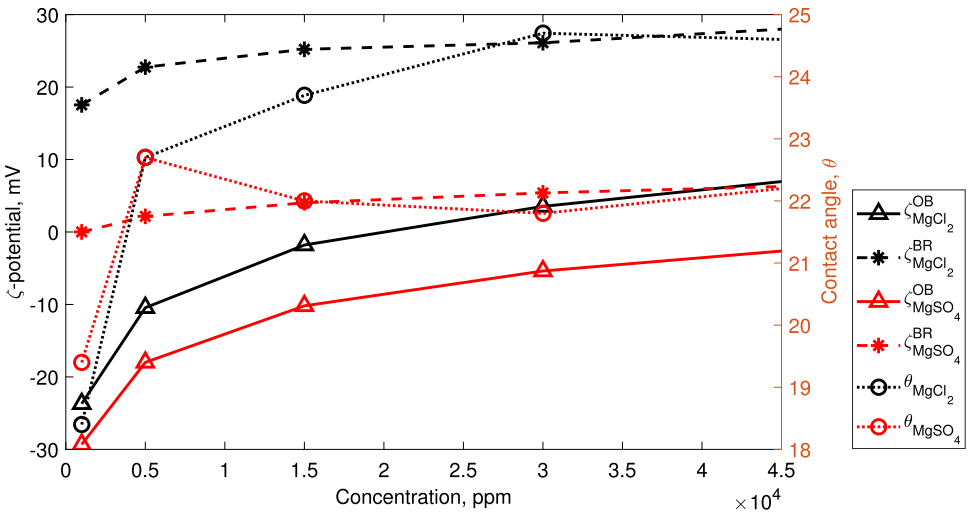

Figure 11. Calculated ζ-potential for chloride and sulfate salts of magnesium ions (Mg^{2+}) at the crude oil–brine and brine–rock interfaces, as a function of salinity.

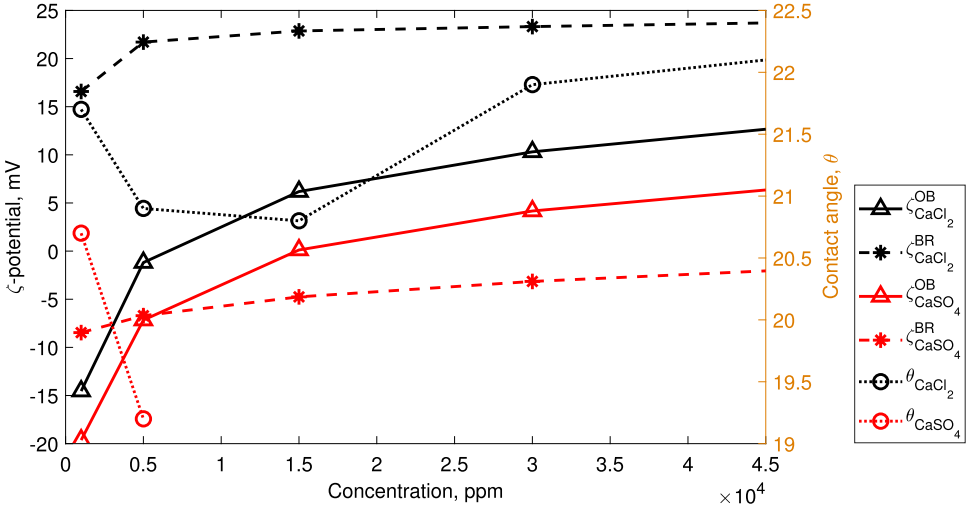

Figure 12. Calculated ζ-potential for chloride and sulfate salts of the calcium ion (Ca^{2+}) at the crude oil–brine and brine–rock interfaces, as a function of salinity.

https://doi.org/10.1021/acs.energyfuels.2c02513
Energy Fuels 2023, 37, 175−190

AUTHOR INFORMATION

Corresponding Authors

Bamikole J. Adeyemi − *School of Engineering, University of Aberdeen, King's College, Aberdeen AB24 3UE, U.K.;* orcid.org/0000-0002-7734-3357; Email: koleadeyemi247@yahoo.com

Prashant Jadhawar − *School of Engineering, University of Aberdeen, King's College, Aberdeen AB24 3UE, U.K.;* orcid.org/0000-0002-2049-0460; Email: prashant.jadhawar@abdn.ac.uk

Author

Lateef Akanji − *School of Engineering, University of Aberdeen, King's College, Aberdeen AB24 3UE, U.K.;* orcid.org/0000-0001-5158-6134

Complete contact information is available at: https://pubs.acs.org/10.1021/acs.energyfuels.2c02513

Notes

The authors declare no competing financial interest.

ACKNOWLEDGMENTS

The authors thank the Petroleum Technology Development Fund (PTDF), Nigeria for funding this project.

REFERENCES

(1) Zhang, L.; Yue, X.; Guo, F. Micro-mechanisms of residual oil mobilization by viscoelastic fluids. *Pet. Sci.* **2008**, *5*, 56−61.

(2) McGuire, P. L.; Chatham, J. R.; Paskvan, F. K.; Sommer, D. M.; Carini, F. H. In *Low Salinity Oil Recovery: An Exciting New EOR Opportunity for Alaska's North Slope*, SPE Western Regional Meeting, OnePetro, 2005.

(3) Zhang, Y.; Morrow, N. R. In *Comparison of Secondary and Tertiary Recovery With Change in Injection Brine Composition for Crude-Oil/Sandstone Combinations*, SPE/DOE Symposium on Improved Oil Recovery, OnePetro, 2006.

(4) Zhang, P.; Tweheyo, M. T.; Austad, T. Wettability alteration and improved oil recovery by spontaneous imbibition of seawater into chalk: Impact of the potential determining ions Ca2+, Mg2+, and SO42-. *Colloids Surf., A* **2007**, *301*, No. 271384.

(5) Al-Shalabi, E. W.; Sepehrnoori, K. A comprehensive review of low salinity/engineered water injections and their applications in sandstone and carbonate rocks. *J. Pet. Sci. Eng.* **2016**, No. 271812.

(6) Sheng, J. J. Critical review of low-salinity waterflooding. *J. Pet. Sci. Eng.* **2014**, No. 271812.

(7) Tang, G.-Q.; Morrow, N. R. Influence of brine composition and fines migration on crude oil/brine/rock interactions and oil recovery. *J. Pet. Sci. Eng.* **1999**, No. 271812.

(8) Ding, H.; Rahman, S. Experimental and theoretical study of wettability alteration during low salinity water flooding-an state of the art review. *Colloids Surf., A* **2017**, *520*, No. 271384.

(9) RezaeiDoust, A.; Puntervold, T.; Strand, S.; Austad, T. Smart Water as Wettability Modifier in Carbonate and Sandstone: A Discussion of Similarities/Differences in the Chemical Mechanisms. *Energy Fuels* **2009**, *23*, 4479−4485.

(10) Roof, J. G. Snap-Off of Oil Droplets in Water-Wet Pores. *Soc. Pet. Eng. J.* **1970**, *10*, 85−90.

(11) Dang, C. T. Q.; Nghiem, L. X.; Chen, Z.; Nguyen, Q. P.; Nguyen, N. T. B. In *State-of-the Art Low Salinity Waterflooding for Enhanced Oil Recovery*, SPE Asia Pacific Oil and Gas Conference and Exhibition, OnePetro, 2013.

(12) Bidhendi, M. M.; Garcia-Olvera, G.; Morin, B.; Oakey, J. S.; Alvarado, V. Interfacial Viscoelasticity of Crude Oil/Brine: An Alternative Enhanced-Oil-Recovery Mechanism in Smart Water-flooding. *SPE J.* **2018**, *23*, 803−818.

(13) Buckley, J. S.; Takamura, K.; Morrow, N. R. Influence of Electrical Surface Charges on the Wetting Properties of Crude Oils. *SPE Reservoir Eng.* **1989**, *4*, 332−340.

(14) Hirasaki, G. J. In *Wettability: Fundamentals and Surface Forces*, SPE Formation Evaluation, SPE-17367-PA, OnePetro, 1991.

(15) Dehghan Monfared, A.; Ghazanfari, M. H.; Jamialahmadi, M.; Helalizadeh, A. Adsorption of silica nanoparticles onto calcite: Equilibrium, kinetic, thermodynamic and DLVO analysis. *Chem. Eng. J.* **2015**, *281*, 334−344.

(16) Bai, H. J.; Lassabatere, L.; Lamy, E. Colloid Transport in Aggregated Porous Media with Intra- and Interaggregate Porosities. *Ind. Eng. Chem. Res.* **2018**, *57*, 6553−6567.

(17) Caetano, D. L. Z.; de Carvalho, S. J.; Metzler, R.; Cherstvy, A. G. Critical adsorption of multiple polyelectrolytes onto a nanosphere: splitting the adsorption−desorption transition boundary. *J. R. Soc., Interface* **2020**, *17*, No. 20200199.

(18) Cherstvy, A. G.; Winkler, R. G. Strong and weak adsorptions of polyelectrolyte chains onto oppositely charged spheres. *J. Chem. Phys.* **2006**, *125*, No. 064904.

(19) Metin, C. O.; Lake, L. W.; Miranda, C. R.; Nguyen, Q. P. Stability of aqueous silica nanoparticle dispersions. *J. Nanopart. Res.* **2011**, *13*, 839−850.

(20) Sadeqi-Moqadam, M.; Riahi, S.; Bahramian, A. An investigation into the electrical behavior of oil/water/reservoir rock interfaces: The implication for improvement in wettability prediction. *Colloids Surf., A* **2016**, *490*, 268−282.

(21) Alshakhs, M. J.; Kovscek, A. R. Understanding the role of brine ionic composition on oil recovery by assessment of wettability from colloidal forces. *Adv. Colloid Interface Sci.* **2016**, *233*, 126−138.

(22) Jackson, M. D.; Al-Mahrouqi, D.; Vinogradov, J. Zeta potential in oil-water-carbonate systems and its impact on oil recovery during controlled salinity water-flooding. *Sci. Rep.* **2016**, *6*, No. 37363.

(23) Lee, K. S.; Lee, J. H.*Hybrid Enhanced Oil Recovery using Smart Waterflooding*, Lee, K. S.; Lee, J. H., Eds.; Gulf Professional Publishing, 2019; pp 27−37.

(24) Mahani, H.; Keya, A. L.; Berg, S.; Bartels, W.-B.; Nasralla, R.; Rossen, W. R. Insights into the Mechanism of Wettability Alteration by Low-Salinity Flooding (LSF) in Carbonates. *Energy Fuels* **2015**, *29*, 1352−1367.

(25) Tian, H.; Wang, M. Electrokinetic mechanism of wettability alternation at oil-water-rock interface. *Surf. Sci. Rep.* **2017**, *72*, 369−391.

(26) Gregory, J. Approximate expressions for retarded van der waals interaction. *J. Colloid Interface Sci.* **1981**, *83*, 138−145.

(27) Sanaei, A.; Sepehrnoori, K. In *Implication of Oil/Brine/Rock Surface Interactions in Modeling Modified Salinity Waterflooding in Carbonate and Sandstone Reservoirs*, SPE Annual Technical Conference and Exhibition, OnePetro, 2018.

(28) Fuller, G. G.; Vermant, J. Complex Fluid-Fluid Interfaces: Rheology and Structure. *Annu. Rev. Chem. Biomol. Eng.* **2012**, *3*, 519−543.

(29) Al-Shalabi, E. W.; Sepehrnoori, K. A comprehensive review of low salinity/engineered water injections and their applications in sandstone and carbonate rocks. *J. Pet. Sci. Eng.* **2016**, *139*, 137−161.

(30) Ruecker, M.; Berg, S.; Armstrong, R.; Georgiadis, A.; Ott, H.; Schwing, A.; Neiteler, R.; Brussee, N.; Makurat, A.; Leu, L.; Wolf, M.; Khan, F.; Enzmann, F.; Kersten, M. From connected pathway flow to ganglion dynamics: Ganglion Dynamics. *Geophys. Res. Lett.* **2015**, *42*, 8.

(31) Awolayo, A. N.; Sarma, H. K.; Nghiem, L. X. Modeling the characteristic thermodynamic interplay between potential determining ions during brine-dependent recovery process in carbonate rocks. *Fuel* **2018**, *224*, 701−717.

(32) Boampong, L. O.; Rafati, R.; Haddad, A. S. A calibrated surface complexation model for carbonate-oil-brine interactions coupled with reservoir simulation—Application to controlled salinity water flooding. *J. Pet. Sci. Eng.* **2022**, *208*, No. 109314.

(33) Bonto, M.; Eftekhari, A. A.; Nick, H. Y. In *A Mechanistic Model for the Fines-Migration During the Modified-salinity Waterflooding in*

Carbonate Reservoirs, IOR 2019−20th European Symposium on Improved Oil Recovery, European Association of Geoscientists & Engineers, 2019; pp 1−18.
(34) Bonto, M.; Eftekhari, A. A.; Nick, H. In *A Calibrated Model for the Carbonate-Brine-Crude Oil Surface Chemistry and its Effect on the Rock Wettability, Dissolution, and Mechanical Properties*, SPE Reservoir Simulation Conference, OnePetro, 2019.
(35) Bordeaux-Rego, F.; Mehrabi, M.; Sanaei, A.; Sepehrnoori, K. Improvements on modelling wettability alteration by Engineered water injection: Surface complexation at the oil/brine/rock contact. *Fuel* **2021**, *284*, No. 118991.
(36) Brady, P. V.; Krumhansl, J. L.; Mariner, P. E. In *Surface Complexation Modeling for Improved Oil Recovery*, SPE Improved Oil Recovery Symposium, OnePetro, 2012.
(37) Brady, P. V.; Thyne, G. Functional Wettability in Carbonate Reservoirs. *Energy Fuels* **2016**, *30*, 9217−9225.
(38) Chandrasekhar, S.; Sharma, H.; Mohanty, K. K. Dependence of wettability on brine composition in high temperature carbonate rocks. *Fuel* **2018**, *225*, 573−587.
(39) Elakneswaran, Y.; Shimokawara, M.; Nawa, T.; Takahashi, S. In *Surface Complexation and Equilibrium Modelling for Low Salinity Waterflooding in Sandstone Reservoirs*, Abu Dhabi International Petroleum Exhibition & Conference, OnePetro, 2017.
(40) Evje, S.; Hiorth, A.A Mathematical Model for Dynamic Wettability Alteration Controlled by Water-Rock Chemistry, 2010. http://aimsciences.org//article/id/d16f3f56-0ff3-494a-b344-b2a4afb18b51.
(41) Fjelde, I.; Asen, S. M.; Omekeh, A.; Polanska, A. In *Secondary and Tertiary Low Salinity Water Floods: Experiments and Modeling*, EAGE Annual Conference & Exhibition Incorporating SPE Europec, SPE-164920-MS, OnePetro, 2013.
(42) Gopani, P. H.; Singh, N.; Sarma, H. K.; Mattey, P.; Srivastava, V. R. Role of Monovalent and Divalent Ions in Low-Salinity Water Flood in Carbonate Reservoirs: An Integrated Analysis through Zeta Potentiometric and Simulation Studies. *Energies* **2021**, *14*, No. 729.
(43) Kazemi Nia Korrani, A.; Sepehrnoori, K.; Delshad, M. Coupling IPhreeqc with UTCHEM to model reactive flow and transport. *Comput. Geosci.* **2015**, *82*, 152−169.
(44) Korrani, A. K. N.; Jerauld, G. R. Modeling wettability change in sandstones and carbonates using a surface-complexation-based method. *J. Pet. Sci. Eng.* **2019**, *174*, 1093−1112.
(45) Omekeh, A.; Friis, H. A.; Fjelde, I.; Evje, S. In *Modeling of Ion-Exchange and Solubility in Low Salinity Water Flooding*, SPE Improved Oil Recovery Symposium 2012, SPE-154144-MS, OnePetro, 2012.
(46) Qiao, C.; Johns, R.; Li, L. Modeling Low-Salinity Waterflooding in Chalk and Limestone Reservoirs. *Energy Fuels* **2016**, *30*, 884−895.
(47) Qiao, C.; Johns, R.; Li, L. In *Understanding the Chemical Mechanisms for Low Salinity Waterflooding*, 78th EAGE Conference and Exhibition 2016, SPE-180138-MS, OnePetro, 2016.
(48) Rahnemaie, R.; Hiemstra, T.; van Riemsdijk, W. H. Inner- and outer-sphere complexation of ions at the goethite−solution interface. *J. Colloid Interface Sci.* **2006**, *297*, 379−388.
(49) Romanuka, J.; Hofman, J.; Ligthelm, D. J.; Suijkerbuijk, B.; Marcelis, F.; Oedai, S.; Brussee, N.; der Linde van; Aksulu, H.; Austad, T. In *Low Salinity EOR in Carbonates*, SPE Improved Oil Recovery Symposium, SPE-153869-MS, OnePetro, 2012.
(50) Sanaei, A.; Varavei, A.; Sepehrnoori, K. Mechanistic modeling of carbonated waterflooding. *J. Pet. Sci. Eng.* **2019**, *178*, 863−877.
(51) Takeya, M.; Shimokawara, M.; Elakneswaran, Y.; Nawa, T.; Takahashi, S. Predicting the electrokinetic properties of the crude oil/brine interface for enhanced oil recovery in low salinity water flooding. *Fuel* **2019**, *235*, 822−831.
(52) Takeya, M.; Ubaidah, A.; Shimokawara, M.; Okano, H.; Nawa, T.; Elakneswaran, Y. Crude oil/brine/rock interface in low salinity waterflooding: Experiments, mathematical model-layer surface complexation model, and DLVO theory. *J. Pet. Sci. Eng.* **2020**, *188*, No. 106913.
(53) Shalabi, E. W. A.; Sepehrnoori, K.Modeling of the LSWI/EWI Technique in Sandstones and Carbonates. In *Low Salinity and Engineered Water Injection for Sandstone and Carbonate Reservoirs*, Walid Al Shalabi, E.; Sepehrnoori, K., Eds.; Gulf Professional Publishing, 2017; Chapter 5, pp 51−71.
(54) Xie, Q.; Sari, A.; Pu, W.; Chen, Y.; U Brady, P.; Maskari, N. A.; Saeedi, A. pH effect on wettability of oil/brine/carbonate system: Implications for low salinity water flooding. *J. Pet. Sci. Eng.* **2018**, *168*, 419−425.
(55) Hilfer, R.; Doster, F. Generalized Buckley Leverett theory for two-phase flow in porous media. *New J. Phys.* **2011**, *13*, No. 123030.
(56) Smith, G. E. In *Waterflooding Heavy Oils*, SPE Rocky Mountain Regional Meeting, OnePetro, 1992.
(57) Rauscher, M.; MAunch, A.; Wagner, B.; Blossey, R. A thin-film equation for viscoelastic liquids of Jeffreys type. *Eur. Phys. J. E* **2005**, *17*, 373−379.
(58) Barra, V.; Afkhami, S.; Kondic, L. Interfacial dynamics of thin viscoelastic films and drops. *J. Non-Newtonian Fluid Mech.* **2016**, *237*, 26−38.
(59) De Wit, A.; Gallez, D.; Christov, C. I. Nonlinear evolution equations for thin liquid films with insoluble surfactants. *Phys. Fluids* **1994**, *6*, 3256−3266.
(60) Kasmaei, A. K.; Rao, D. N. In *Is Wettability Alteration the Main Cause for Enhanced Recovery in Low-Salinity Waterflooding?*, SPE Reservoir Evaluation & Engineering, SPE-169120-MS, OnePetro, 2014.
(61) Karoussi, O.; Hamouda, A. A. Imbibition of Sulfate and Magnesium Ions into Carbonate Rocks at Elevated Temperatures and Their Influence on Wettability Alteration and Oil Recovery. *Energy Fuels* **2008**, *22*, 2129−2130.
(62) Hamouda, A. A.; Karoussi, O. Effect of Temperature, Wettability and Relative Permeability on Oil Recovery from Oil-wet Chalk. *Energies* **2008**, *1*, 19−34.
(63) Hamouda, A. A.; Gomari, K. A. R. In *Influence of Temperature on Wettability Alteration of Carbonate Reservoirs*, SPE/DOE Symposium on Improved Oil Recovery, SPE-99848-MS, OnePetro, 2006.
(64) Alotaibi, M. B.; Nasralla, R. A.; Nasr-El-Din, H. A. In *Wettability Challenges in Carbonate Reservoirs*, SPE Improved Oil Recovery Symposium, SPE-129972-MS, OnePetro, 2010.
(65) Fernø, M. A.; Gronsdal, R.; Asheim, J.; Nyheim, A.; Berge, M.; Graue, A. Use of Sulfate for Water Based Enhanced Oil Recovery during Spontaneous Imbibition in Chalk. *Energy Fuels* **2011**, *25*, 1697−1706.
(66) Kasha, A.; Al-Hashim, H.; Abdallah, W.; Taherian, R.; Sauerer, B. Effect of Ca2+, Mg2+ and SO42- ions on the zeta potential of calcite and dolomite particles aged with stearic acid. *Colloids Surf., A* **2015**, *482*, 290−299.
(67) Chen, Y.; Xie, Q.; Sari, A.; U Brady, P.; Saeedi, A. Oil/water/rock wettability: Influencing factors and implications for low salinity water flooding in carbonate reservoirs. *Fuel* **2018**, *215*, 171−177.
(68) Rezaei Gomari, K.; Hamouda, A. A. Effect of fatty acids, water composition and pH on the wettability alteration of calcite surface. *J. Pet. Sci. Eng.* **2006**, *50*, 140−150.
(69) Mahani, H.; Keya, A. L.; Berg, S.; Nasralla, R. Electrokinetics of Carbonate/Brine Interface in Low-Salinity Waterflooding: Effect of Brine Salinity, Composition, Rock Type, and pH on zeta-Potential and a Surface-Complexation Model. *SPE J.* **2016**, *22*, 53−68.
(70) Yousef, A. A.; Al-Saleh, S.; Al-Jawfi, M. In *New Recovery Method for Carbonate Reservoirs through Tuning the Injection Water Salinity: Smart WaterFlooding*, SPE EUROPEC/EAGE Annual Conference and Exhibition, OnePetro, 2011.
(71) Lashkarbolooki, M.; Riazi, M.; Hajibagheri, F.; Ayatollahi, S. Low salinity injection into asphaltenic-carbonate oil reservoir, mechanistical study. *J. Mol. Liq.* **2016**, *216*, 377−386.
(72) Vijapurapu, C. S.; Rao, D. N. In *Effect of Brine Dilution and Surfactant Concentration on Spreading and Wettability*, International Symposium on Oilfield Chemistry, SPE-80273-MS, OnePetro, 2003.
(73) Meng, W.; Haroun, M. R.; Sarma, H. K.; Adeoye, J. T.; Aras, P.; Punjabi, S.; Rahman, M. M.; Kobaisi, M. A. In *A Novel Approach of Using Phosphate-spiked Smart Brines to Alter Wettability in Mixed Oil-*

https://doi.org/10.1021/acs.energyfuels.2c02513
Energy Fuels 2023, 37, 175−190

wet Carbonate Reservoirs, Abu Dhabi International Petroleum Exhibition and Conference, OnePetro, 2015.
(74) Boinovich, L.; Emelyanenko, A. Wetting and surface forces. *Adv. Colloid Interface Sci.* **2011**, *165*, 60−69.
(75) Derjaguin, B.; Landau, L. The theory of stability of highly charged lyophobic sols and coalescence of highly charged particles in electrolyte solutions. *Acta Physicochim. URSS* **1941**, *14*, No. 58.
(76) Derjaguin, B.; Landau, L. Theory of stability of highly charged liophobic sols and adhesion of highly charged particles in solutions of electrolytes. *Zh. Eksperim. i Teor. Fiz.* **1945**, *15*, 663−682.
(77) Verwey, E. J. W. Theory of the stability of lyophobic colloids. *J. Phys. Chem. A* **1947**, *51*, 631−636.
(78) Basu, S.; Sharma, M. M. Measurement of Critical Disjoining Pressure for Dewetting of Solid Surfaces. *J. Colloid Interface Sci.* **1996**, *181*, 443−455.
(79) Taheriotaghsara, M.; Bonto, M.; Nick, H. M.; Eftekhari, A. A. Estimation of calcite wettability using surface forces. *J. Ind. Eng. Chem.* **2021**, *98*, 444−457.
(80) Teletzke, G. F.; Ted Davis, H.; Sciven, L. E. How liquids spread on solids. *Chem. Eng. Commun.* **1987**, *55*, 41−82.
(81) Diez, J. A.; Kondic, L. On the breakup of fluid films of finite and infinite extent. *Phys. Fluids* **2007**, *19*, No. 072107.
(82) Seric, I.; Afkhami, S.; Kondic, L. Interfacial instability of thin ferrofluid films under a magnetic field. *J. Fluid Mech.* **2014**, *755*, R1.
(83) Adeyemi, B.; Jadhawar, P.; Akanji, L.; Barra, V. Effects of fluid-fluid interfacial properties on the dynamics of bounded viscoelastic thin liquid films. *J. Non-Newtonian Fluid Mech.* **2022**, *309*, No. 104893.
(84) Gumerman, R. J.; Homsy, G. M. The Stability of Radially Bounded Thin Films. *Chem. Eng. Commun.* **1975**, *2*, 27−36.
(85) Lashkarbolooki, M.; Ayatollahi, S.; Riazi, M. The impacts of aqueous ions on interfacial tension and wettability of an asphaltenic-acidic crude oil reservoir during smart water injection. *J. Chem. Eng. Data* **2014**, *59*, 3624−3634.
(86) Bird, R. B.; Armstrong, R. C.; Hassager, O.*Dynamics of Polymeric Liquids, Vol. 1 Fluid Mechanics Vol. 22*; Wiley Interscience, 1987.
(87) Tomar, G.; Shankar, U.; Shukla, S. K.; Sharma, A.; Biswas, G. Instability and dynamics of thin viscoelastic liquid films. *Eur. Phys. J. E* **2006**, *20*, 185−200.
(88) Tewari, R. D.; Dandekar, A. Y.; Ortiz, J. M.*Petroleum Fluid Phase Behavior: Characterization, Processes, and Applications*; CRC Press, 2018.
(89) Takamura, K.; Chow, R. S. A Mechanism For Initiation of Bitumen Displacement From Oil Sand. *J. Can. Pet. Technol.* **1983**, *22*, 10.
(90) Mugele, F.; Bera, B.; Cavalli, A.; Siretanu, I.; Maestro, A.; Duits, M.; Cohen-Stuart, M.; van den Ende, D.; Stocker, I.; Collins, I. Ion adsorption-induced wetting transition in oil-water-mineral systems. *Sci. Rep.* **2015**, *5*, No. 10519.
(91) Fathi, S. J.; Austad, T.; Strand, S. Smart Water as a Wettability Modifier in Chalk: The Effect of Salinity and Ionic Composition. *Energy Fuels* **2010**, *24*, 2514−2519.
(92) Shaik, I.; Song, J.; Biswal, S.; Hirasaki, G.; Bikkina, P.; Aichele, C. Effect of brine type and ionic strength on the wettability alteration of naphthenic-acid-adsorbed calcite surfaces. *J. Pet. Sci. Eng.* **2020**, *185*, No. 106567.
(93) Yousef, A. A.; Al-Saleh, S.; Al-Jawfi, M. In *Improved/Enhanced Oil Recovery from Carbonate Reservoirs by Tuning Injection Water Salinity and Ionic Content*, SPE Improved Oil Recovery Symposium, OnePetro, 2012.
(94) Liu, J.; Wani, O. B.; Alhassan, S. M.; Pantelides, S. T. Wettability Alteration and Enhanced Oil Recovery Induced by Proximal Adsorption of $\{Na\}^{+}$, $\{Cl\}^{-}$, $\{Ca\}^{2+}$, $\{Mg\}^{2+}$, and $\{SO\}_4^{2-}$ Ions on Calcite. *Phys. Rev. Appl.* **2018**, *10*, No. 034064.
(95) Yousef, A. A.; Al-Saleh, S.; Al-Kaabi, A.; Al-Jawfi, M. In *Laboratory Investigation of Novel Oil Recovery Method for Carbonate Reservoirs*, Canadian Unconventional Resources and International Petroleum Conference, SPE-137634-MS, OnePetro, 2010.
(96) Aslan, S.; Najafabadi, N. F.; Firoozabadi, A. Non-monotonicity of the Contact Angle from NaCl and MgCl2 Concentrations in Two Petroleum Fluids on Atomistically Smooth Surfaces. *Energy Fuels* **2016**, *30*, 2858−2864.
(97) Chandrasekhar, S.; Mohanty, K. K. In *Wettability Alteration with Brine Composition in High Temperature Carbonate Reservoirs*, SPE Annual Technical Conference and Exhibition, OnePetro, 2013.

https://doi.org/10.1021/acs.energyfuels.2c02513
Energy Fuels 2023, 37, 175−190